Korean J. Chem. Eng., 37(12), 2104-2116 (2020)
DOI: 10.1007/s11814-020-0634-y

pISSN: 0256-1115
eISSN: 1975-7220

Effects of heat sink structure on heat transfer performance cooled by semiconductor and nanofluids

Cong Qi*,,†, Tiantian Chen*,**, Jianglin Tu*,**, and Yuxing Wang*,****

*Jiangsu Province Engineering Laboratory of High Efficient Energy Storage Technology and Equipments, China University of Mining and Technology, Xuzhou 221116, China
**School of Electrical and Power Engineering, China University of Mining and Technology, Xuzhou 221116, China
(*Received 28 March 2020 • Revised 13 June 2020 • Accepted 11 July 2020*)

Abstract−On account of the low heat dissipation problem of common cooling systems, an experimental system with enhanced structures was set to improve the heat transfer of heat sink cooled by semiconductor and TiO_2-water nanofluids. The influences of structures (smooth surface, metal foam with PPI=30, cylindrical bulge (height: H=2 mm, staggered arrangement), cylindrical groove (depth: D′=2 mm, staggered arrangement)), nanoparticle mass fractions (ω= 0.0-0.5 wt%), input power of the semiconductor (P=2 W, 4 W, 6 W), and Reynolds numbers (Re=414-1,119) on the flow and heat transfer properties of TiO_2-water nanofluids were studied. The compositive thermal and hydraulic properties of the enhanced technologies were analyzed by thermal efficiency. Results indicated that the combination of semiconductor and metal foam shows the most excellent performance compared with other combinations and it can be enhanced by 48.1% at best. Nanofluids with ω=0.4 wt% display the best cooling capacity instead of the highest concentration. The cooling effect shows an increasing trend with the input power of the semiconductor.

Keywords: Nanofluids, Heat Sink, Semiconductor, Thermal Efficiency

INTRODUCTION

With the rapid development of computers, the heat dissipation problems of the heat sink also increase more than ever. The previous ways of heat dissipation no longer meet the requirements of the high heat flow density, and the high temperature will reduce the performance of the heat sink and even the burning phenomenon will appear. Given the heat dissipation problem, two effective methods can be taken in terms of the structure of equipment and working media. Compared with ordinary coolant, on one hand, nanoparticles can increase the thermal conductivity of the original pure liquid and enhance the heat transfer process. At the same particle volume content, the surface area of nanoparticles is much larger than that of millimeter or micrometer particles, so the effective thermal conductivity of nanofluids is greater than that of common two-phase mixture with millimeter or micrometer particles. On the other hand, the large Brown force of nanoparticles can obviously improve the heat transfer. Hence, nanofluids can significantly improve cooling efficiency and heat dissipation. The heat conductivity of the emerging nanofluids is higher, which significantly improves cooling efficiency and heat dissipation. Under the same heat transfer volume, nanofluids can transfer more heat, which makes a crucial contribution to improving the compactness and miniaturization of the heat exchangers. Hence, nanofluids are studied by researchers in many fields. Chen et al. [1,2] demonstrated that the solar absorption of SiO_2@Au is related with the core-shell proportion and mixing proportion of diverse nanofluids; meanwhile, particle concentration is also an advantageous factor to enhance the photothermal conversion efficiency of nanofluids. Xuan et al. [3,4] proposed that nanofluids offer a huge potential in heat transfer. Li et al. [5] revealed that Ag@TiO_2 nanofluids have high photothermal conversion efficiency and have advantages in the application field of solar collectors. Hu et al. [6] showed that the concentration of silica nanofluids and particle size have a positive effect on heat transfer, which is conducive to the augment of the physical property of the heat storage media. Nanofluids, as the cooling media [7-9], are widely applied in the heat transfer field. Researchers have already investigated nanofluid performance from the angle of types [10,11], temperatures [12,13], physical properties [14-16], and thermal conductivity [17,18] in recent years.

Impacts of diverse reinforced heat exchange tubes on the heat transfer were investigated, for instance, double-pipe [19], circular tube [20], horizontal tube [21], sinusoidal minitube [22], wavy microchannel [23]. Furthermore, many investigators conducted numerous researches on natural convection and turbulent convection. Shahsavar et al. [24] demonstrated that mixed nanofluids (Fe_3O_4 and carbon nanotubes (CNTs)), whose proportions are 0.9 wt% and 1.35 wt% respectively, can improve the average Nusselt number significantly. Izadi et al. fully discussed the natural convection of various nanofluids in diverse enclosures, such as a vertical shaped [25], a C-shaped [26], a square [27], and a porous enclosure [28, 29]. Natural convection heat transfer, which has low energy consumption and low noise, cannot satisfy the high intensity of heat dissipation. Sheikholeslami et al. discussed the turbulent flow of diverse nanofluids in a circular pipe with helical turbulators [30], a double-pipe [31], a pipe with twisted tape [32,33], and a storage

†To whom correspondence should be addressed.
E-mail: qicong@cumt.edu.cn

enclosure [34]. It was determined that revolution angle, pitch ratio, twisted tape are conducive to reinforcing the intensity of heat transfer. Nasiri et al. [35] revealed the mechanisms of Al_2O_3/H_2O and TiO_2/H_2O nanofluids at the turbulent flow state, and concluded that the accumulated concentrations within a certain range are conducive to strengthening the capacity of heat transfer. Yang et al. [36] researched the six-bladed impeller for turbulent flow of a single and mixing phase in the stirred tank and discovered that the fluid disturbance can be enhanced by the impellers.

In terms of the structural optimization of heat transfer, the heat dissipation problems of heat sinks have already become a research focus. Qi et al. researched the influences of hemispheric bulges [37], rectangular grooves [38], cylindrical grooves [39] on the heat sink heat dissipation characteristics, and conclusions all showed that the heat transfer capacities of the optimized structures are stronger than that of the smooth surface. Dehghan et al. [40] discovered that the addition of porous materials in the heat sink can strengthen the heat transfer. Chen et al. [41] chose different size working media to enhance the exchange efficiency of the microchannel. Shojaeian et al. [42] investigated the structure effect of a parallel surface microchannel, and the viscous dissipation and magnetic field are the innovative factors for the thermal management of the microchannel. Porous medium, as a burgeoning material, has excellent physical properties on heat exchange, especially metal foam. Sardari et al. [43-45] analyzed the diverse metal foam materials from the aspects of the porosity and pore density. It was discovered that metal foam can be applied to the areas of the thermal storages and heat exchangers. Naphon et al. [46,47] investigated the cooling system of a mini-rectangular fin heat sink and a vapor chamber with jet liquid, respectively. Results provided some guidance for the cooling system, which can enhance the cooling performance of the electronic equipment.

Semiconductor refrigeration, also known as thermoelectric refrigeration, is a new pattern of refrigeration technology. Compared with traditional refrigeration, semiconductor refrigeration has no refrigerants and complex mechanical equipment, it has no noise and vibration, and is environmentally friendly. Semiconductor refrigeration has a great development prospect in the industrial field, electronic field, and automatic control field. Furthermore, diverse semiconductor nanofluids were prepared [48,49], and they can be used in the medical field.

The above references show that many researches focus on the influences of nanofluid variety and microchannel structures on the cooling characteristics of the heat sink by a large margin. However, the effects of the semiconductor on the heat sink with enhanced structures are less studied. To reveal the coupling cooling mechanism of three kinds of enhanced heat transfer technologies (semiconductor, heat sink structure and nanofluids), the effects of heat sink structure on heat transfer performance cooled by semiconductor and nanofluids are investigated in this paper. Results of this paper can promote the application of semiconductors in the cooling field of electronic components, optimize the structure of a heat sink and select the most suitable nanofluid composition to achieve the best cooling performance. To accommodate the heat dissipation of the CPU, a square heat sink was chosen. In addition, to further enhance the heat transfer, some enhanced structures (metal foam, cylindrical bulge, cylindrical groove) are used in the heat sink. The major innovations are mainly as below: A semiconductor is applied to the heat sink cooling, which provides a new cooling method for the electron component. Effects of three different enhanced structures (metal foam, cylindrical bulge, cylindrical groove) on the heat sink cooling performance are discussed and the results are also compared with a smooth surface in this paper; meanwhile, the consequences are beneficial to the design and operation of heat sink cooling systems. The structure optimization of the heat sink coupled with the technology of semiconductor can provide a new research direction for microchannel cooling and heat dissipation, and it can be also applied to some large-scale integrated circuits, power components and equipment cooling.

BASIC RESEARCHES

1. Experimental Set

As is known, the choices of fluid media and heat transfer equipment are particularly significant in the field of heat transfer. TiO_2 nanoparticles have extraordinary physical and chemical properties and are widely applied to photocatalysis, solar heat collection, coated materials, and aerospace. An emerging medium (TiO_2-water nanofluids) was chosen in this experiment. The size of the nanoparticles was 10 nm. Compared with the previous microchannel devices, the structural design of the heat sink in this paper was optimized, and the upper side of the cavity was provided with a semiconductor. The type of the selected semiconductor refrigeration chip was TEC1-12715, semiconductor refrigeration chip, also known as thermoelectric refrigeration chip which is a heat pump and a tool for heat transfer. Semiconductor refrigeration equipment is small, so it is easy to maintain and simple to operate. Also, the semiconductor is noiseless and low-cost, and it can control the temperature accurately, adapt to the various environments and own good adaptability.

Fig. 1 displays the experimental setup for the heat sink cooled by TiO_2-H_2O nanofluids and semiconductors. The experimental equipment principally comprises the heat transfer test portion, flow resistance test portion, and cooling installation. Considering that laminar flow is safe and quiet, Reynolds numbers (Re=414-1,119) were chosen and the heat transfer effect was not obvious at low Reynolds number; hence, more smaller Reynolds numbers were not chosen. Reynolds numbers were adjusted by the peristaltic pump with a speed regulation function, the flow range was 20-190 ml/min and the error accuracy was less than 0.5%. The specific operation steps were the same as the previous research [50]. Table 1 displays the detailed information of the equipment. The inlet and outlet of cooling fluid through the heat sink are on the left and right side. In the experiment, the silicon heating sheet was used to simulate heating (heating error is ±0.1 °C). The heating power was provided by a DC power supply. Beyond that, the cold interface of the refrigeration chip takes away the heat of the cavity and releases it to the environment on the other side. In the process of refrigeration, the heat density at the hot side is very large. If the heat is not released in time, it will have a great negative impact on the refrigeration of the refrigeration chip. For the sake of strengthening the convection heat dissipation, an air fan was arranged on the hot

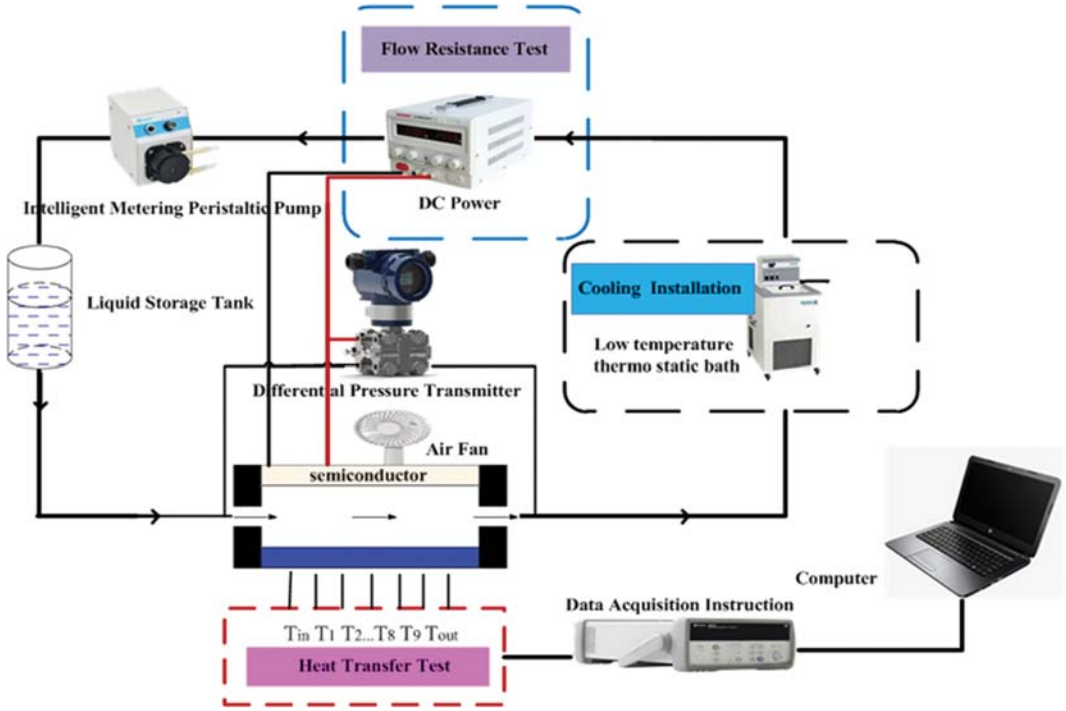

Fig. 1. System schematic diagram.

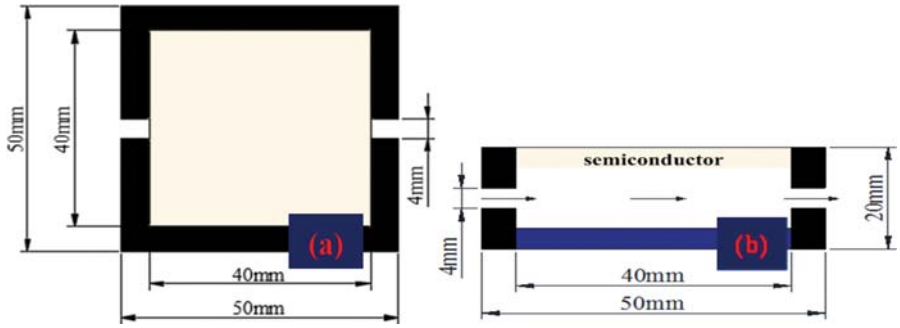

Fig. 2. Particulars of the heat sink, (a) plan elevation, (b) front elevation.

Table 1. Detailed information of the key equipment

Equipment	Feature
Pressure transmitter	Range: 60 pa-40 Mpa Accuracy: 0.25%
Thermocouple	Model: T type Range: 0-200 °C Accuracy: ±0.1%
Data acquisition instrument	Accuracy: 0.004%
Float-type flow meter	Accuracy: ±0.05%

side of the semiconductor, which can accelerate the airflow speed to achieve timely heat dissipation. Fig. 2 displays the detailed structure of the miniature device in this experimental system. For the purpose of comparing the cooling effect of semiconductor coupling with different structure heat sinks, Fig. 3 shows the smooth copper surface, copper metal foam (PPI (pore density inch) is 30 and

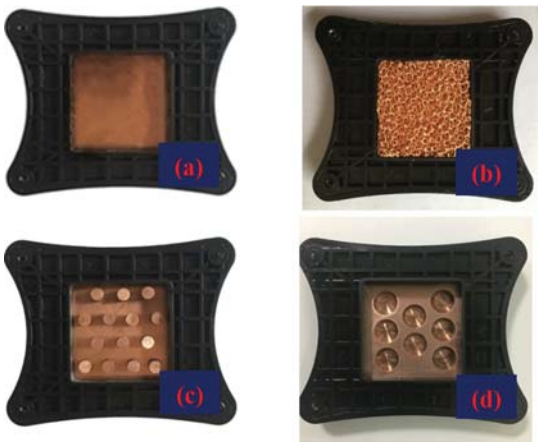

Fig. 3. Particulars of the heat sink, (a) smooth surface, (b) metal foam with PPI=30, (c) cylindrical bulge (H=2 mm, staggered arrangement), (d) cylindrical groove (D′=2 mm, staggered arrangement).

porosity is 90%), staggered arrangement bulges and grooves whose height and depth are all 2 mm. Furthermore, the wall temperature was measured by nine patch thermocouples, and the inlet and outlet temperature were measured by two armored thermocouples.

2. Data Cleansing

The hydraulic diameter is:

$$D=\frac{4A}{L} \tag{1}$$

The specific heat capacity and density of nanofluids are [51]:

$$c_{pnf}=(1-\varphi)c_{pbf}+\varphi c_{pnp} \tag{2}$$

$$\rho_{nf}=(1-\varphi)\rho_{bf}+\varphi\rho_{np} \tag{3}$$

Connection between volume fraction and mass fraction is:

$$\varphi=\frac{1}{(1/\omega)(\rho_{np}/\rho_{nf})} \tag{4}$$

Heat absorption of nanofluids is:

$$Q_{nf}=c_{pnf}q_{nf}(T_{out}-T_{in}) \tag{5}$$

The temperature of the outside surface is:

$$T_{wo}=\frac{(T_1+T_2+\cdots+T_9)}{9} \tag{6}$$

The temperature of the inside surface is:

$$T_{win}=T_{wo}-\frac{Q_{nf}\delta}{A\lambda_w} \tag{7}$$

The average temperature of nanofluids is:

$$T_{nf}=\frac{(T_{out}+T_{in})}{2} \tag{8}$$

Convective heat transfer coefficient is:

$$h=\frac{Q_{nf}}{A(T_{win}-T_{nf})} \tag{9}$$

Nusselt number is:

$$Nu=\frac{h\cdot D}{\lambda_{nf}} \tag{10}$$

Reynolds number is:

$$Re=\frac{\rho_{nf}uD}{\mu_{nf}} \tag{11}$$

Resistance coefficient is reckoned as:

$$f=\frac{2D}{\rho_{nf}u^2}\cdot\frac{\Delta p}{\Delta l} \tag{12}$$

The compositive assessment exponent (thermal efficiency) is [52]:

$$\eta=\left(\frac{Nu_{nf}}{Nu_{bf}}\right)\Big/\left(\frac{f_{nf}}{f_{bf}}\right)^{\frac{1}{3}} \tag{13}$$

3. Analysis of Uncertainty

The uncertainty of the experiment is of great necessity to be analyzed, and the equations for Nu and f are severally [53]:

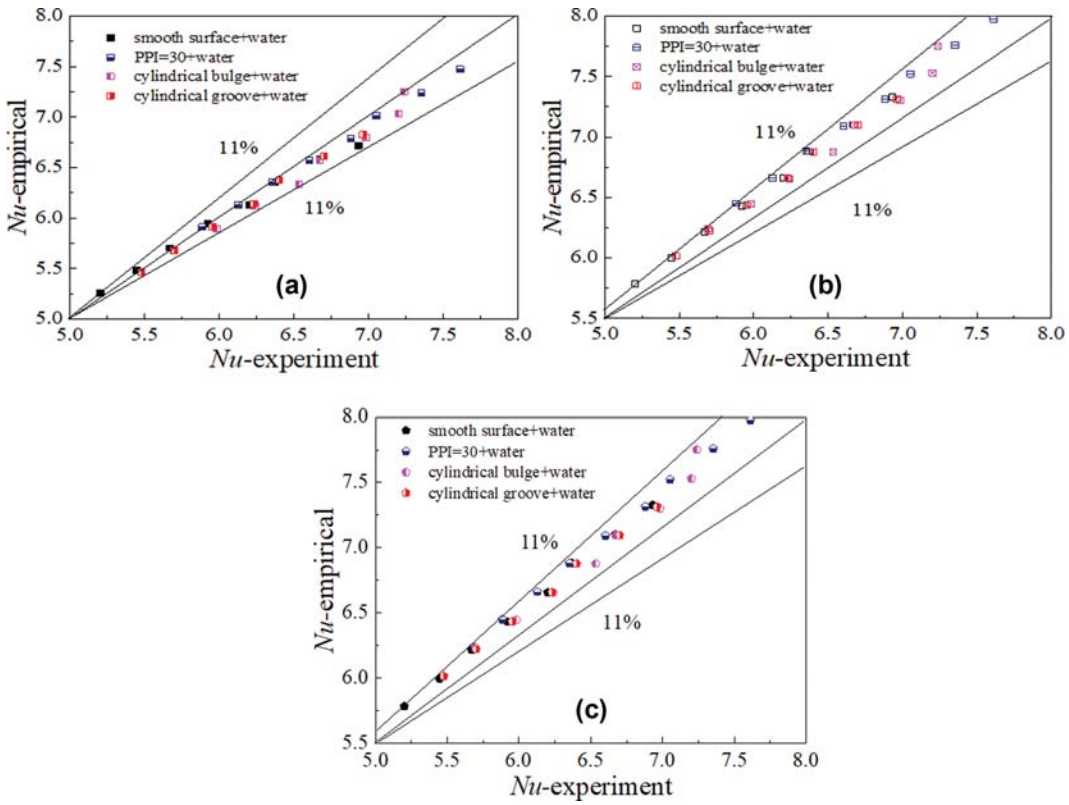

Fig. 4. Comparison between the Nu and that computed by the empirical Eq. (18), (a) P=2 W, (b) P=4 W, (c) P=6 W.

Table 2. Uncertainties of variables

Variables	Q_f	T	p	q_{nf}	l
Uncertainties	±5.0%	±0.1%	±0.5 wt%	±1.06%	±0.1%

$$\frac{\delta Nu}{Nu}=\sqrt{\left(\frac{\delta Q_f}{Q_f}\right)^2+\left(\frac{\delta T}{T}\right)^2} \tag{14}$$

$$\frac{\delta f}{f}=\sqrt{\left(\frac{\delta p}{p}\right)^2+\left(\frac{\delta l}{l}\right)^2+\left(\frac{\delta q_{nf}}{q_{nf}}\right)^2} \tag{15}$$

Table 2 displays the uncertainties of variables in the experiment. The errors of Nu and f are approximately ±5.00% and ±1.176% severally on the basis of Eqs. (14) and (15); the calculated results can make sure the precision of the experimental equipment, which raises the credibility of the system as well.

4. Experimental System Validation

The dependability of the experimental equipment must be verified. The comparison between the Nu in the article and the empirical result is calculated by the Eq. (16) as given in Fig. 4 and the empirical formula is [54]:

$$Nu=0.566(1+100\varphi)^{0.57}Re^{0.20}Pr^{0.18} \tag{16}$$

In Fig. 4, the allowable range of deviation between the experimental result and the empirical value is 11%, and the compared results display that the experimental data in this article are reasonable.

RESULTS AND DISCUSSION

1. Effect of Nanoparticle Mass Fraction

The heat transfer and flow performance of nanofluids in four diverse heat sinks with a semiconductor were studied. Fig. 5 shows that the wall temperature of semiconductor heat sink varies with Reynolds number at diverse nanoparticle mass fractions. Clearly, high Re is beneficial to decreasing the wall temperature, and it may be interpreted that the high Re can result in the distinct disturbance of flow. Moreover, at the same circumstance of input power, the wall temperatures of the semiconductor heat sink decrease with the increase of the concentration when ω=0.0-0.4%, but ω=0.5% is disadvantageous to reduce the wall temperatures. When the concentration of nanofluids increases, viscosity plays a leading role at this point. This means that the concentration should be controlled within a reasonable range. For ω=0.0-0.4%, the thermal conductivity is improved after adding nanoparticles into the base solution, and meanwhile the Brownian motion of the nanofluids im-

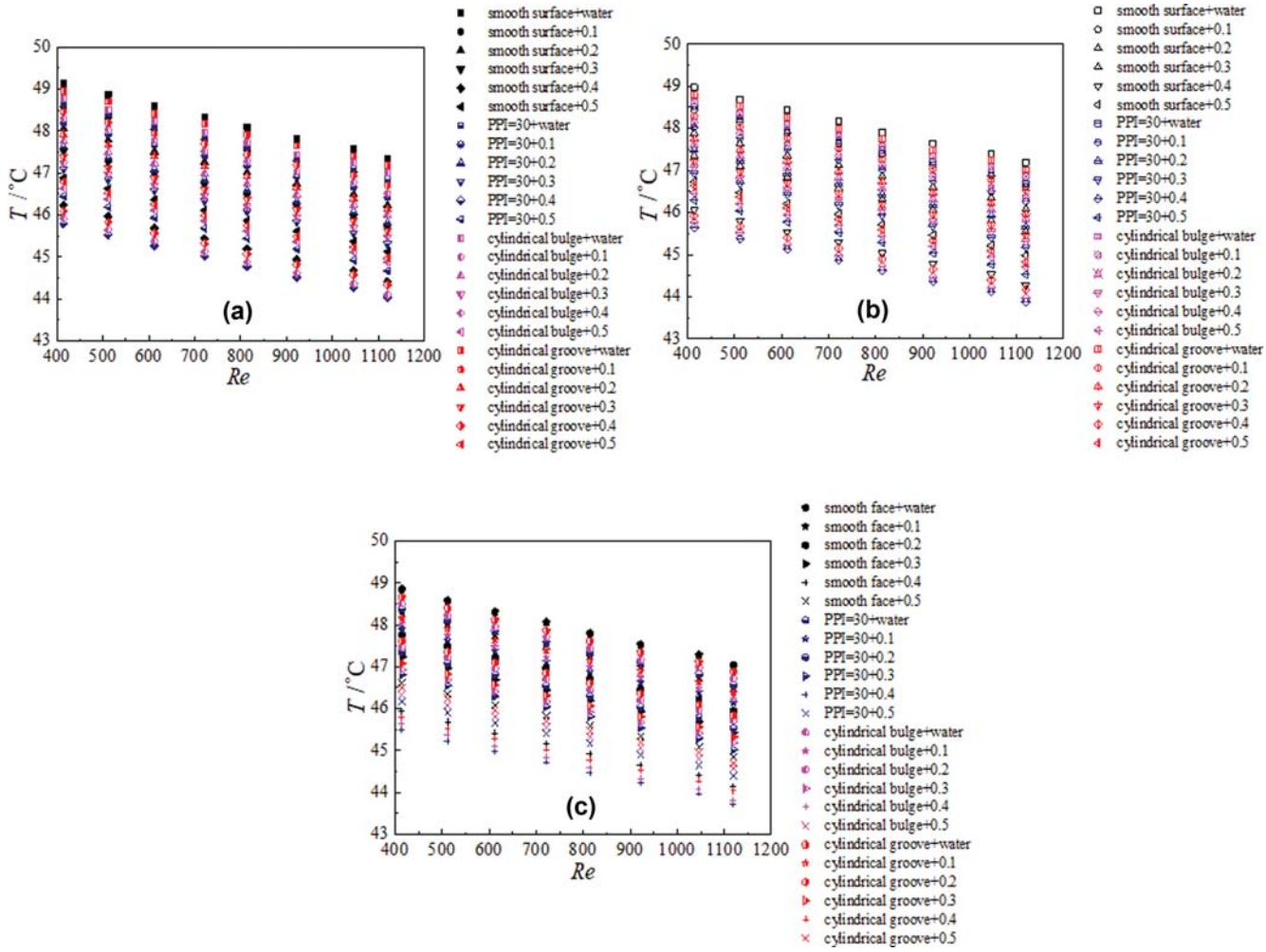

Fig. 5. Impact of nanoparticle mass fraction on temperature, (a) P=2 W, (b) P=4 W, (c) P=6 W.

proves the heat transfer capability. Hence, nanofluids with ω=0.4% exhibit superior cooling behavior compared with other concentrations. For ω=0.5%, the impact of viscosity is larger than that of thermal conductivity; hence, nanofluids with ω=0.5% begin to reduce the thermal performance.

Also, metal foam with PPI=30 has the best cooling effect under the same input power. The wall temperature of the semiconductor heat sink can be reduced by 6.0% at most in comparison with that with the smooth surface. In comparison with the cylindrical grooves, the T of the semiconductor heat sink with cylindrical bulges can be reduced by 5.7%.

In addition to the influence on wall temperature, the convection heat transfer coefficients and Nusselt numbers under diverse Re are exhibited in Fig. 6 and Fig. 7. The convection heat transfer coefficient and Nusselt number have a positive causal connection with Reynolds numbers, and the analogous reason has been given before. For each of the diverse heat sinks, nanofluids with ω=0.4% indicate the optimal capacity of cooling property, which can be increased by 40.9% in comparison to water at optimal conditions. Besides, the combination of nanofluids with ω=0.4% and metal foam with PPI=30 shows the best capacity of heat transfer. Compared with a smooth surface, the increase proportions in Nusselt number caused by the metal foam with PPI=30, cylindrical bulges, cylindrical grooves can reach up to 6.7%, 4.7%, 2.5% at most under the identical circumstance. For metal foam, it has a high surface area and good physical property (heat dissipation). The porous structure of the metal foam can strengthen the nanofluid mixing, give rise to some vortexes, and weaken the laminar boundary layer, thus bringing about strong convection heat transfer. For cylindrical bulges, the flow direction of fluids is disrupted by the staggered arrangement cylindrical bulges, thus causing some vortexes and strengthening the heat transfer. For cylindrical grooves, some vortexes exist

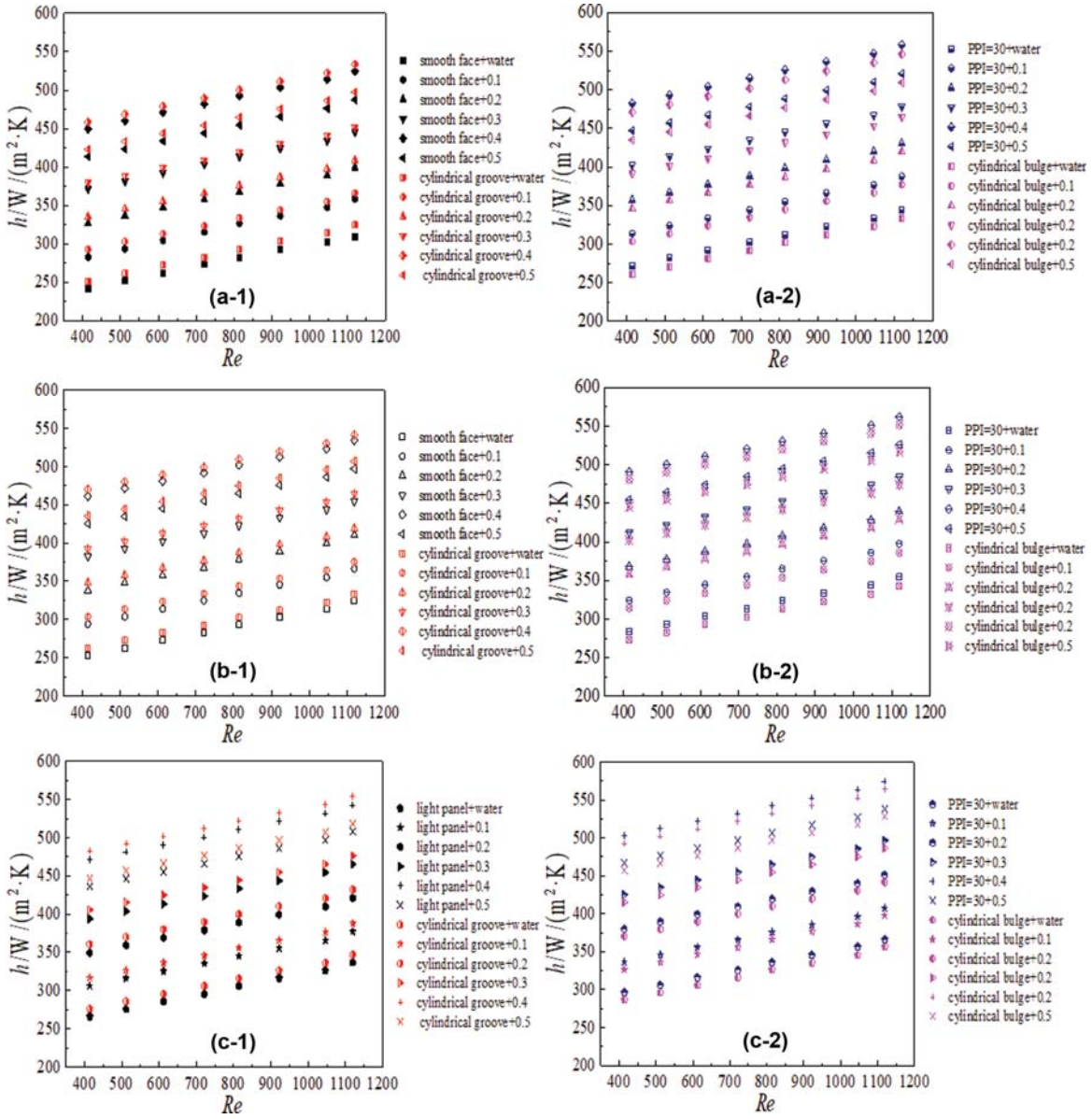

Fig. 6. Impact of nanoparticle mass fraction on convection heat transfer coefficient, (a) P=2 W, (b) P=4 W, (c) P=6 W.

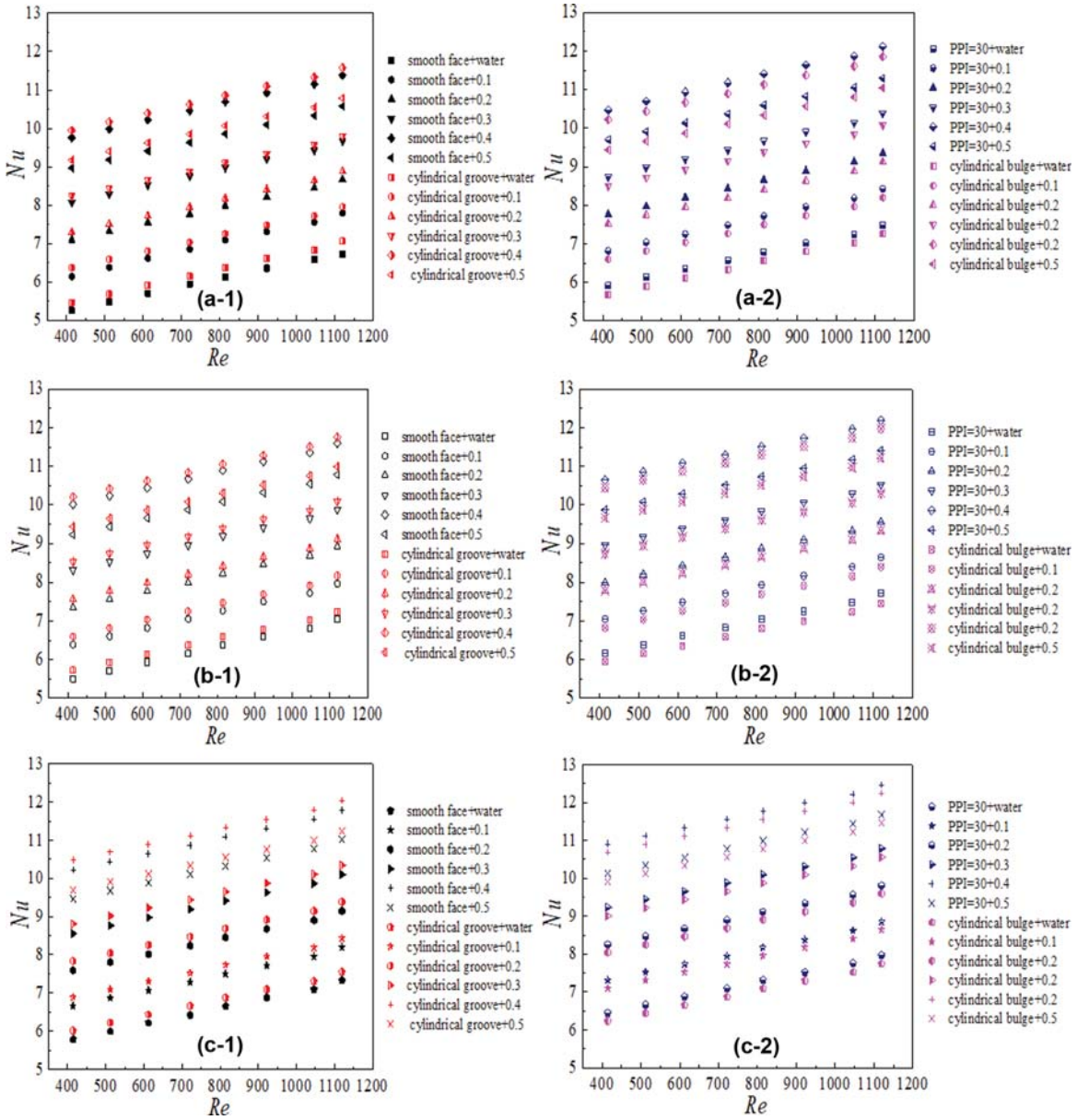

Fig. 7. Impact of nanoparticle mass fraction on Nusselt number, (a) P=2 W, (b) P=4 W, (c) P=6 W.

in the grooves of the copper surface. On one hand, these vortexes can aggravate the disturbance in the grooves; on the other hand, the vortexes in grooves play a rolling bearing role, and the effect of flow drag reduction can be achieved. The heat transfer effect of nanofluids is largely enhanced when they pass through these heat sinks, which manifests that the ingenious design of the heat sink structure is propitious to boost heat transfer to some extent.

The heat transfer can be intensified by the nanofluids, which results from the high thermal conductivity; meanwhile, the increase of resistance coefficient can also result from the rise of mass fractions of nanofluids. The influences of nanoparticle mass fraction on the resistance coefficient are given in Fig. 8; it is obtained that the concentrations give rise to the increase in the flow resistance coefficient. The increase in concentration brings about large viscosity, and the pressure drop also increases. The reason can be explained as that the high viscosity of nanofluids is detrimental to the flow resistance. Furthermore, Stokes forces caused by the velocity between the particles and water molecules can block the flow velocity [55,56]. Fig. 8 also displays that the resistance coefficient of the smooth surface is less than the heat sinks with metal foam, staggered cylindrical bulge, and cylindrical groove. The metal foam has some permeability, which results in the increase of resistance coefficient of the fluid flow. The cylindrical bulge with staggered arrangement can convert the directions of flow tremendously, which can bring about larger turbulence and a higher resistance coefficient. The cylindrical groove can cause some eddies and increase the resistance coefficient.

2. Impact of Semiconductor Power

Besides researching the effect of mass fraction, we also further analyzed the impact of the different input power of semiconductor

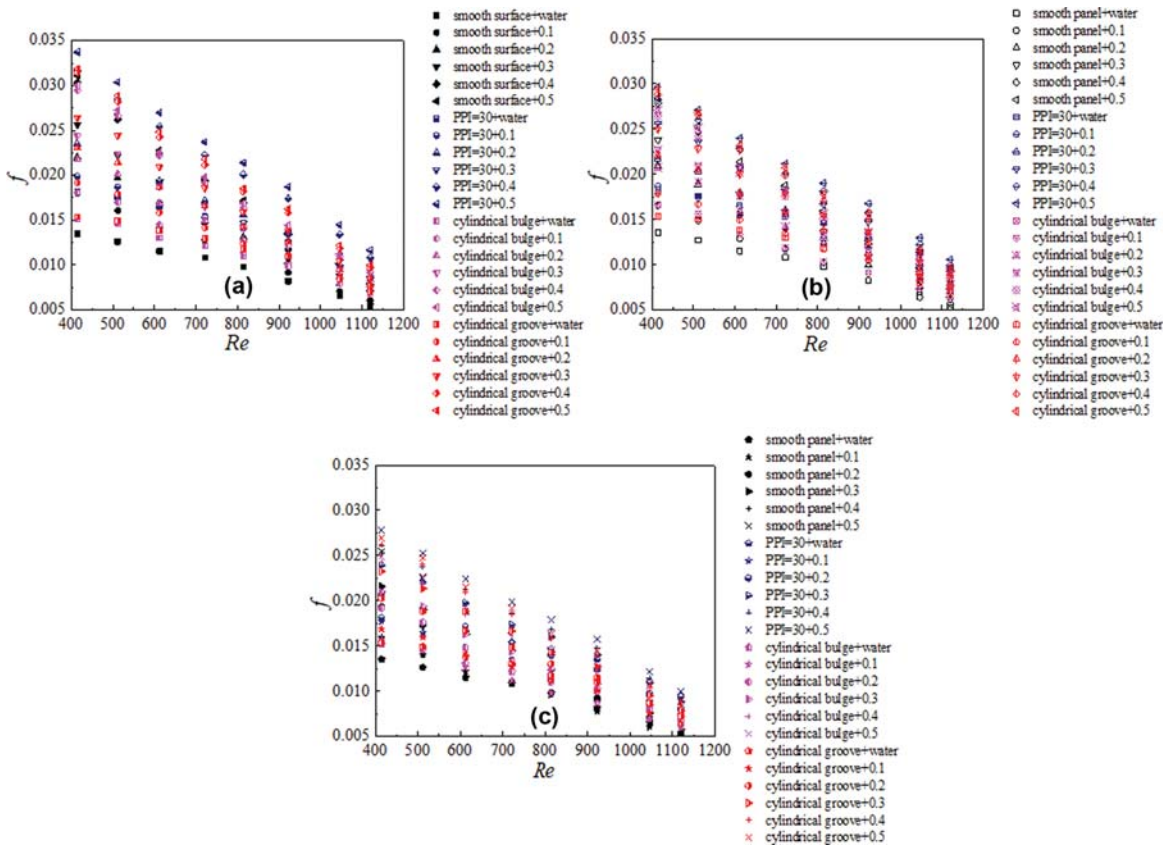

Fig. 8. Impact of nanoparticle mass fraction on resistance coefficient, (a) P=2 W, (b) P=4 W, (c) P=6 W.

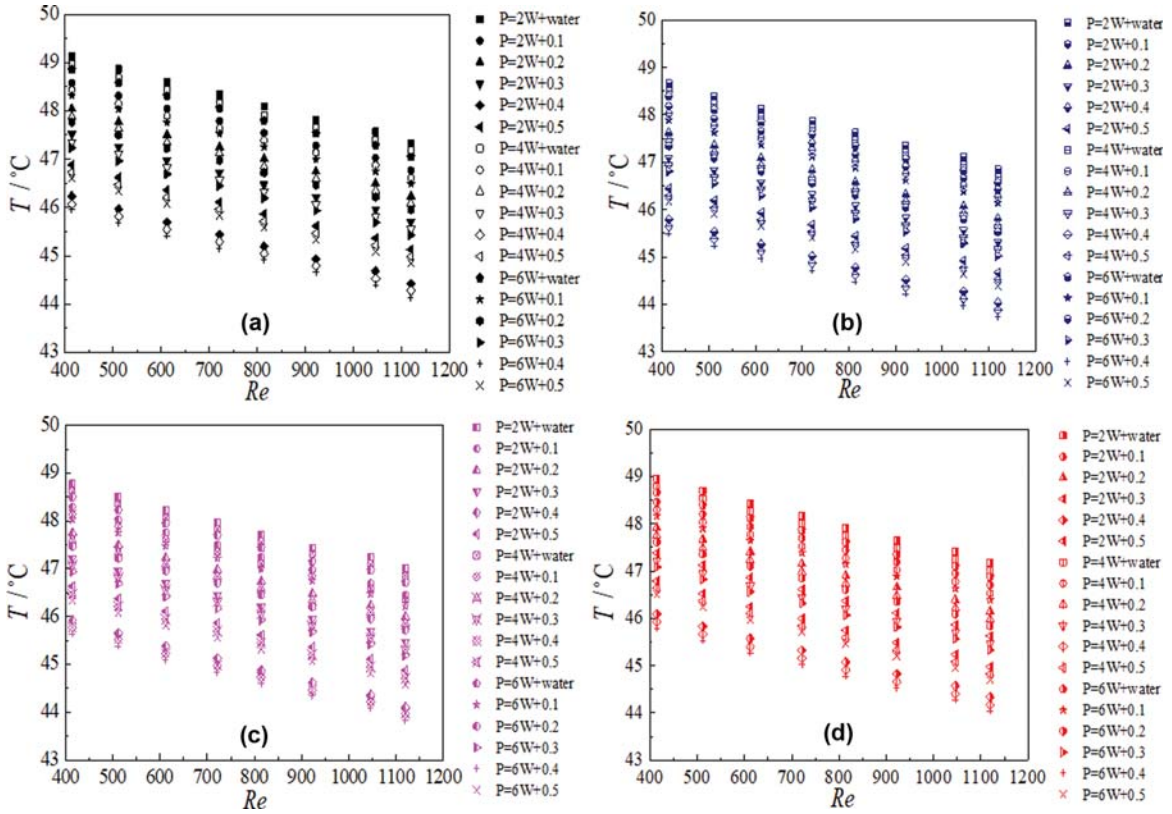

Fig. 9. Impact of power on temperature, (a) smooth surface, (b) metal foam with PPI=30, (c) cylindrical bulge, (d) cylindrical groove.

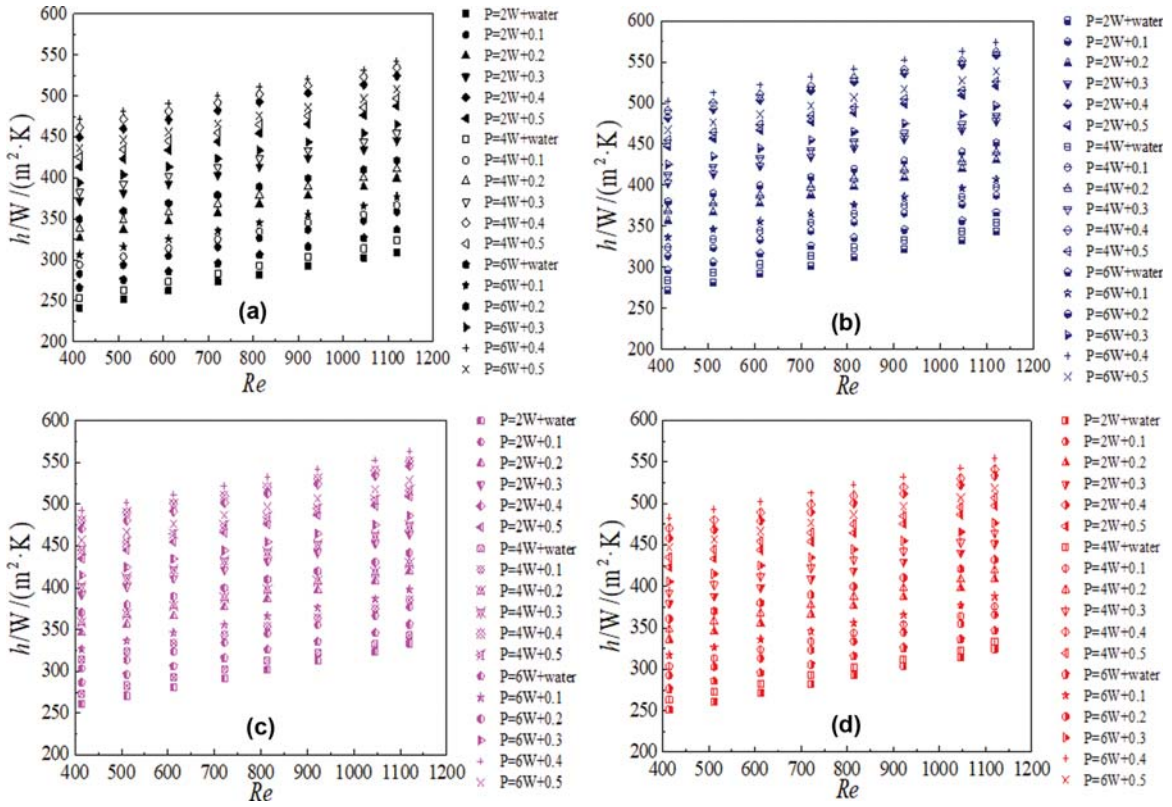

Fig. 10. Impact of power on convection heat transfer coefficient, (a) smooth surface, (b) metal foam with PPI=30, (c) cylindrical bulge, (d) cylindrical groove.

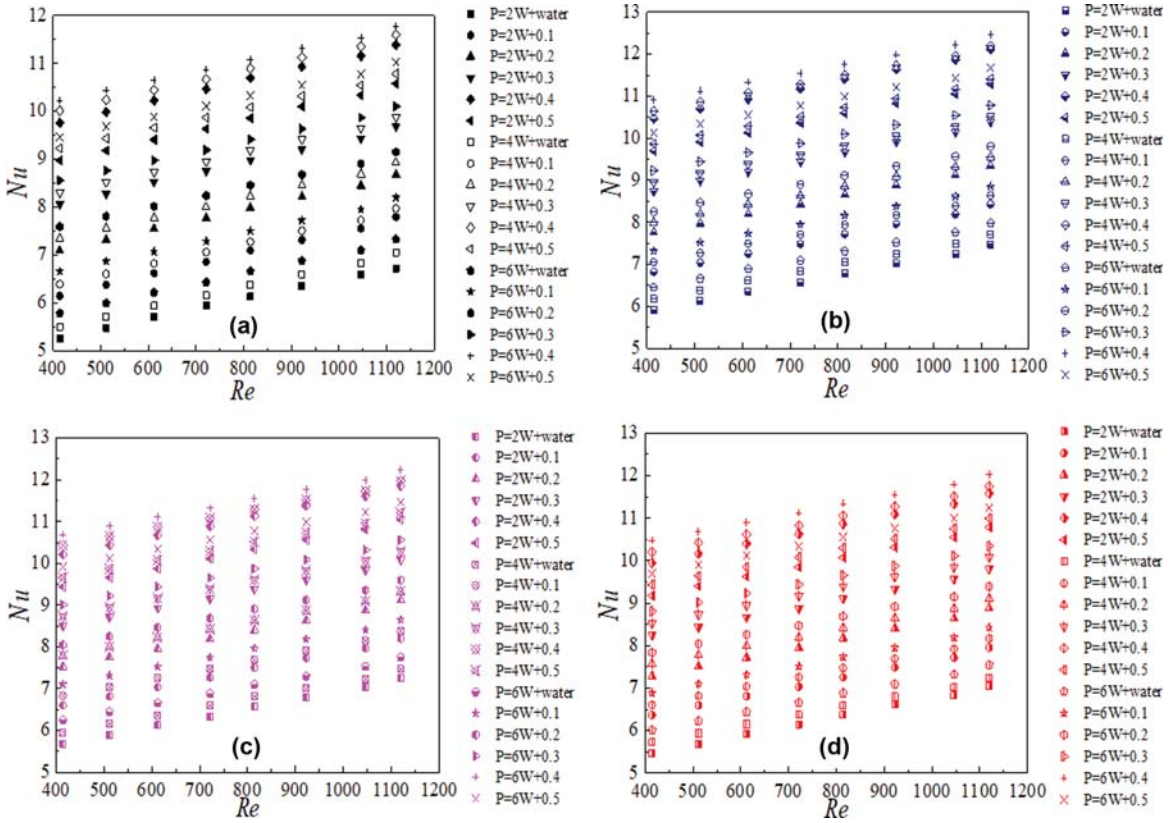

Fig. 11. Impact of power on Nusselt number, (a) smooth surface, (b) metal foam with PPI=30, (c) cylindrical bulge, (d) cylindrical groove.

on the wall temperature, Nusselt number, convection heat transfer coefficient, and resistance coefficient.

The semiconductor refrigeration device is a kind of solid component with high heat flux density, and the refrigeration technology of the semiconductor is relatively simple.

As for the same heat sink, the effects of different heated power on the wall temperature are displayed in Fig. 9. Conclusions were obtained that the wall temperatures reduce with the increase of input power at the same concentrations (ω=0.0-0.5%). It can be interpreted as that the higher input power, the more heat is absorbed by the cold side. The heat absorbed from the cold side (the heat absorption section) of the semiconductor refrigeration component is moved on to the hot side (the heat dissipation section). Then the absorbed heat is dissipated by the hot side of the semiconductor. Increasing the input power of the semiconductor is conducive to reducing the wall temperature of the heat sink, which contributes to the heat dissipation property of the heat sink.

The influence of the different input power of the semiconductor on the h and Nu is given in Fig. 10 and Fig. 11, respectively. Conclusions are obtained that Nu and h inicrease with the semiconductor input power. As for the four heat sinks, the convection heat transfer coefficient at P=6 W is increased by 4.2% and 2.5% compared with that at P=2 W and P=4 W, respectively, at the optimal condition. In addition, the smooth surface, cylindrical bulge, cylindrical groove at P=6 W can increase the Nusselt number by 4.8%, 4.5%, 4.4% at most in comparison with that at P=2 W, respectively. This reveals that the cooling property of the heat sink is boosted by a small increase of the power, and the increasing input power is propitious to strengthening the ability of heat transfer.

3. Compositive Assessment

In addition to the increase in the capability of heat transfer, the enhanced technologies also cause an increase in the pressure drop.

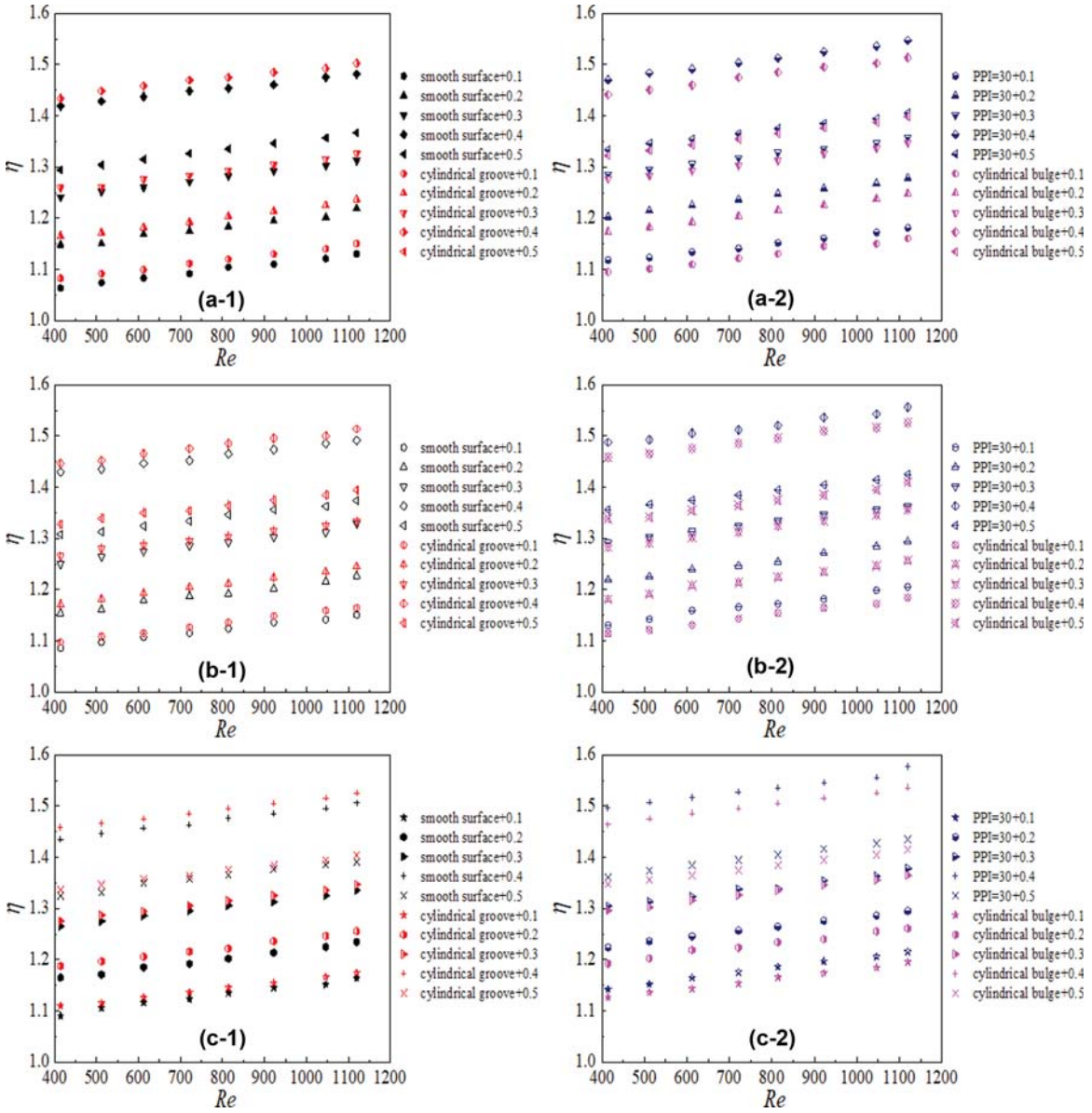

Fig. 12. Thermal efficiency compositive assessment, (a) P=2 W, (b) P=4 W, (c) P=6 W.

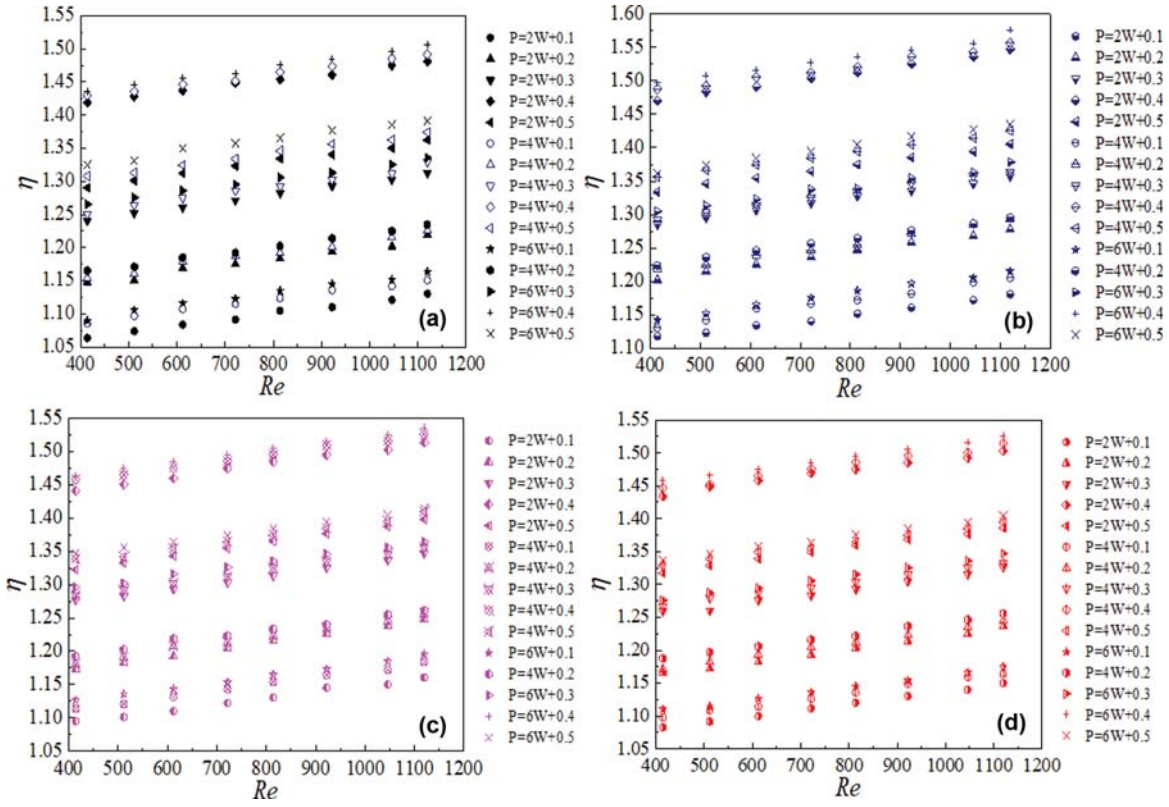

Fig. 13. Impacts of input power on thermal efficiency compositive assessment exponent, (a) smooth surface, (b) metal foam with PPI=30, (c) cylindrical bulge, (d) cylindrical groove.

To make the most suitable choice, a compositive performance exponent is necessary to assess the heat transfer and pressure drop.

The compositive assessment computed by Eq. (13) is used to appraise the flow and thermal performances, and the results are in Fig. 12. The tendency of compositive performance keeps pace with Nusselt number. The mass fraction range from ω=0.0% to 0.4% can improve the compositive performance exponent. However, the nanofluids ω=0.5% deteriorates the heat transfer, and it is because that viscosity plays a blocking influence. Compared to the heat sink with the smooth surface, the compositive performance of metal foam with PPI=30, cylindrical bulge and cylindrical groove can be increased by 4.6%, 2.3%, 1.6%, respectively. Furthermore, Fig. 13 shows the impact of input power on the thermal efficiency compositive assessment exponent, and results indicate that the compositive assessment exponent increases with the input power of semiconductor. The reason is similar to that of Fig. 12 and Fig. 13, which have been explained in detail before. For a smooth surface, metal foam, cylindrical bulge and cylindrical groove, the semiconductor with P=6 W shows the highest thermal efficiency exponent which can reach 1.51, 1.58, 1.54, 1.53, respectively.

CONCLUSIONS

An experimental study was conducted to investigate the effects of the semiconductor input power on thermal-hydraulic properties of nanofluids in a heat sink on the basis of thermal efficiency. Some main conclusions are presented below:

(1) Nanofluids with ω=0.4 wt% display the best cooling capacity instead of the highest concentration.

(2) The combination of semiconductor and metal foam shows the most excellent performance compared with other combinations and it can be enhanced by 48.1% at best.

(3) The cooling effect shows an increasing trend with the input power of the semiconductor.

(4) Four diverse heat sinks are coupled with a semiconductor cooling technology, which can give guiding significance to the improvement of cooling performance in the heat sink.

(5) Nanoparticle shape may influence the heat transfer. The nanoparticles used in this paper are spherical. However, due to the limitation of the actual preparation process, some particle sizes of the prepared nanoparticles may be not spherical in an absolute sense, which may cause some errors between the results of this paper and others.

(6) Although nanofluids prepared in this work are highly stable, due to various factors in actual operation the stability still affects its wide application. The stability of nanofluids in different environments is still needed to be investigated further.

(7) The future work is to research the impact of larger semiconductor input power on the cooling system. If the heat density is too large and is not dissipated in time, it will have a negative impact on the cooling of electronic components.

ACKNOWLEDGEMENTS

This work is financially supported by Natural Science Founda-

tion of Jiangsu Province, China (Grant No. BK20181359).

NOMENCLATURE

A : area of the copper [m^2]
c_p : specific heat of nanofluids [$J \cdot kg^{-1} \cdot K^{-1}$]
D : hydraulic diameter [m]
D′ : depth of cylindrical groove [m]
f : frictional resistance coefficient
h : convection heat transfer coefficient [$W \cdot m^{-2} \cdot K^{-1}$]
l : length [m]
L : wetted perimeter [m]
Nu : Nusselt number
$\Delta p/\Delta l$: pressure drop per unit length [Pa/m]
PPI : pores per inch
Q : heat absorption of nanofluids [W]
q : mass flow rate [kg/s]
Re : Reynolds number
T : temperatures [K]
u : velocity of nanofluids [m/s]

Greek Symbols

ρ : density [kg/m^3]
φ : volume fraction [%]
ω : mass fraction [%]
δ : thickness of copper [m]
λ : thermal conductivity [$W \cdot m^{-1} \cdot K^{-1}$]
μ : dynamic viscosity [Pa·s]
η : compositive assessment exponent

Subscripts

bf : base fluid
nf : nanofluids
np : nanoparticle
w : wall
in : inlet
out : outlet

REFERENCES

1. M. Chen, Y. He, J. Zhu and D. Wen, *Appl. Energy*, **181**, 65 (2016).
2. M. Chen, Y. He, X. Wang and Y. Hu, *Appl. Energy*, **211**, 735 (2018).
3. Y. Xuan and Q. Li, *Int. J. Heat Fluid Flow*, **21**(1), 58 (2000).
4. X. Fang, Y. Xuan and Q. Li, *Appl. Phys. Lett.*, **95**(20), 203108 (2009).
5. H. Li, Y. He, C. Wang, X. Wang and Y. Hu, *Appl. Energy*, **236**, 117 (2019).
6. Y. Hu, Y. He, Z. Zhang and D. Wen, *Sol. Energy Mat. Sol. Cells*, **192**, 94 (2019).
7. V. Nikkhah, M. M. Sarafraz and F. Hormozi, *Chem. Biochem. Eng. Q.* **29**(3), 405 (2015).
8. A. Arya, M. M. Sarafraz, S. Shahmiri, S. A. Madani, V. Nikkhah and S. M. Nakhjavani, *Heat. Mass Transf.*, **54**(4), 985 (2018).
9. A. Asadi, M. Asadi, A. Rezaniakolaei, L. Rosendahl, M. Afrand and S. Wongwises, *Int. J. Heat Mass Transf.*, **117**, 474 (2018).
10. Z. Li, A. Shahsavar, A. A. Alrashed and P. Talebizadehsardari, *Appl. Therm. Eng.*, **167**, 114777 (2020).
11. R. Zhang, S. Aghakhani, A. H. Pordanjani, S. M. Vahedi, A. Shahsavar and M. Afrand, *Eur. Phys. J Plus.*, **135**(2), 1 (2020).
12. M. Baratpour, A. Karimipour, M. Afrand and S. Wongwises, *Int. Commun. Heat Mass Transf.*, **74**, 108 (2016).
13. S. Atashrouz, M. Mozaffarian and G. Pazuki, *Korean J. Chem. Eng.*, **33**(9), 2522 (2016).
14. A. A. Alrashed, A. Karimipour, S. A. Bagherzadeh, M. R. Safaei and M. Afrand, *Int. J. Heat Mass Transf.*, **127**, 925 (2018).
15. M. Vafaei, M. Afrand, N. Sina, R. Kalbasi, F. Sourani and H. Teimouri, *Phys. E Syst. Nanos.*, **85**, 90 (2017).
16. Z. Li, M. Sheikholeslami, A. J. Chamkha, Z. A. Raizah and S. Saleem, *Comput. Method. Appl. Mech. Eng.*, **338**, 618 (2020).
17. I. Kim, H. Sim, H. Hong, D. Kim, W. Lee and D. Lee, *Korean J. Chem. Eng.*, **36**(6), 1004 (2019).
18. A. Komeilibirjandi, A. H. Raffiee, A. Maleki, M. A. Nazari and M. S. Shadloo, *J. Therm. Anal. Calorim.*, **139**(4), 2679 (2020).
19. M. Hojjat, S. G. Etemad and R. Bagheri, *Korean J. Chem. Eng.*, **27**(5), 1391 (2010).
20. B. Chun, H. U. Kang and S. H. Kim, *Korean J. Chem. Eng.*, **25**(5), 966 (2008).
21. H. I. Mohammed, P. T. Sardari and D. Giddings, *Int. J. Therm. Sci.*, **146**, 106099 (2019).
22. L. Yang, K. Du and Z. Zhang, *Int. J. Mech. Sci.*, **168**, 105310 (2020).
23. H. Bazdar, D. Toghraie, F. Pourfattah, O. A. Akbari, H. M. Nguyen and A. Asadi, *J. Therm. Anal. Calorim.*, **139**(3), 2365 (2020).
24. A. Shahsavar, P. T. Sardari and D. Toghraie, *Int. J. Numer. Meth. Heat Fluid Flow*, **29**(3), 915 (2019).
25. M. Izadi, R. Mohebbi, D. Karimi and M. A. Sheremet, *Chem. Eng. Proc.*, **125**, 56 (2018).
26. R. Mohebbi, M. Izadi and A. J. Chamkha, *Phys. Fluids*, **29**(12), 122009 (2017).
27. S. A. Mehryan, M. Izadi, A. J. Chamkha and M. A. Sheremet, *J. Mol. Liq.*, **263**, 510 (2018).
28. M. Izadi, G. Hoghoughi, R. Mohebbi and M. A. Sheremet, *J. Mol. Liq.*, **261**, 357 (2018).
29. M. Izadi, R. Mohebbi, A. A. Delouei and H. Sajjadi, *Int. J. Mech. Sci.*, **151**, 154 (2019).
30. M. Sheikholeslami, M. Jafaryar and Z. Li, *Int. J. Heat Mass Transf.*, **124**, 980 (2018).
31. M. Sheikholeslami, D. D. Ganji and M. Gorjibandpy, *Appl. Therm. Eng.*, **100**, 805 (2016).
32. M. Sheikholeslami, M. Jafaryar and Z. Li, *J. Mol. Liq.*, **263**, 489 (2018).
33. M. Jafaryar, M. Sheikholeslami, Z. Li and R. Moradi, *J. Therm. Anal. Calorim.*, **135**(1), 305 (2019).
34. Z. Li, M. Sheikholeslami, M. Ayani, M. Shamlooei, A. Shafee, M. Waly and I. Tlili, *Physica A*, **524**, 540 (2019).
35. M. Nasiri, S. G. Etemad and R. Bagheri, *Korean J. Chem. Eng.*, **28**(12), 2230 (2011).
36. F. L. Yang, S. Zhou and C. X. Zhang, *Korean J. Chem. Eng.*, **32**(5), 816 (2015).
37. C. Qi, N. Zhao, X. Cui, T. Chen and J. Hu, *Int. J. Heat Mass Transf.*, **123**, 320 (2018).
38. N. Zhao, L. Guo, C. Qi, T. Chen and X. Cui, *Energy Convers. Manage.*, **181**, 235 (2019).
39. N. Zhao, C. Qi, T. Chen, J. Tang and X. Cui, *Int. J. Heat Mass*

Transf., **135**, 16 (2019).
40. M. Dehghan, M. S. Valipour and S. Saedodin, *Energy Convers. Manage.*, **110**, 22 (2016).
41. J. Chen, J. Han and D. Xu, *Int. J. Hydrogen Energy*, **44**(23), 11546 (2019).
42. M. Shojaeian and S. M. Shojaee, *Korean J. Chem. Eng.*, **30**(4), 823 (2013).
43. P. T. Sardari, D. M. Grant, D. Giddings, G. S. Walker and M. Gillott, *Energy Convers. Manage.*, **201**, 112151 (2019).
44. P. T. Sardari, H. I. Mohammed, D. Giddings, G. S. Walker, M. Gillott and D. M. Grant, *Energy*, **189**, 116108 (2019).
45. P. T. Sardari, D. Giddings, D. M. Grant, M. Gillott and G. S. Walker, Renew. *Energy*, **148**, 987 (2020).
46. P. Naphon, S. Klangchart and S. Wongwises, *Int. Commun. Heat Mass Transf.*, **36**(8), 834 (2009).
47. P. Naphon, *Energy Convers. Manage.*, **48**, 2708 (2007).
48. M. P. Gonzalezaraoz, J. F. Sanchezramirez, J. L. Jimenezperez, E. Chigoanota, J. L. Herreraperez and J. G. Mendozaalvarez, *Nat. Sci.*, **4**(12), 1022 (2012).
49. S. M. S. Murshed, F. J. V. Santos and C. A. de Castro, *J. Nano*, **2**(4), 261 (2013).
50. C. Qi, J. Hu, M. Liu, L. Guo and Z. Rao, *Energy Convers. Manage.*, **153**, 557 (2017).
51. B. C. Pak and Y. I. Cho, *Exp. Heat Transf.*, **11**(2), 151 (1998).
52. C. Qi, Y. Wan, C. Li, D. Han and Z. Rao, *Int. J. Heat Mass Transf.*, **115**(Part B), 1072 (2017).
53. S. Kline, *Mech. Eng.*, **75**, 3 (1953).
54. X. Wu and H. Wu, *J. Chem. Ind. Eng. (in Chinese)*, **59**(9), 2181 (2008).
55. C. Qi, L. Liang and Z. Rao, *Int. J. Heat Mass Transf.*, **94**, 316 (2016).
56. C. Qi, G. Wang, L. Yang, Y. Wan and Z. Rao, *Int. J. Heat Mass Transf.*, **105**, 664 (2017).